# Please cite the Published Version

Khan, Muhzamil A. , Bernalte, Elena , Whittingham, Matthew J. , Slimani, Lilian, Augusto, Karen K. L. , Crapnell, Robert D. and Banks, Craig E. (2025) Laser-Engraved Print Beds for Creating Bespoke Surface Architectures on Additive Manufactured Electrodes. ChemElectroChem. e202500234 ISSN 2196-0216

DOI: https://doi.org/10.1002/celc.202500234

Publisher: Wiley

Version: Published Version

Downloaded from: https://e-space.mmu.ac.uk/641829/

Usage rights: Creative Commons: Attribution 4.0

**Additional Information:** This is an open access article published in ChemElectroChem, by Wiley. **Data Access Statement:** The data that support the findings of this study are available from the

corresponding author upon reasonable request.

# **Enquiries:**

If you have questions about this document, contact openresearch@mmu.ac.uk. Please include the URL of the record in e-space. If you believe that your, or a third party's rights have been compromised through this document please see our Take Down policy (available from https://www.mmu.ac.uk/library/using-the-library/policies-and-guidelines)



www.chemelectrochem.org

# Laser-Engraved Print Beds for Creating Bespoke Surface Architectures on Additive Manufactured Electrodes

Muhzamil A. Khan, Elena Bernalte, Matthew J. Whittingham, Lilian Slimani, Karen K. L. Augusto, Robert D. Crapnell,\* and Craig E. Banks\*

Moving from planar electrodes to unique surface architectures can produce significant improvements in electrochemical performance. Herein, we report the inclusions of unique microstructures fabricated onto the electrode surface through printing them onto laser-engraved print beds modified with different patterns (lines, crosses, circles, waves, and unmodified surfaces). Unique surface architectures were successfully produced on the surface of additive manufactured working electrodes printed from both commercial and bespoke conductive poly(lactic acid) and bespoke poly(propylene) (B-PP) filaments. Within both poly(lactic acid) filaments, minimal alteration in performance was seen, proposed to be due to the ingress of solution negating the surface architecture. For the B-PP, which do not suffer from

solution ingress, significant improvements in peak current and electrochemical area were found for all surface architectures against both inner and outer sphere redox probes, with a cross architecture producing the largest improvement. This was corroborated in the electroanalytical application, with electrodes with crosses surface architecture producing a 3-fold improvement in sensitivity, limit of detection, and limit of quantification when compared to electrodes with no additional surface architecture for the detection of acetaminophen. This work shows improvements in the electrochemical performance of additive manufactured electrodes can be achieved through simply modifying the print bed, without alterations to print files or post-print modification methods.

#### 1. Introduction

The interaction between redox molecules and the surface of electrodes is fundamental to the performance of electroanalytical sensing platforms. Even so, the vast majority of electrode surfaces are produced to be planar surfaces, allowing for simple elucidation of areas and processes. Although still useful, these systems are not optimized for the maximum electroanalytical performance possible. By transitioning from planar working electrode surfaces to unique surface architectures, it is possible to maximize

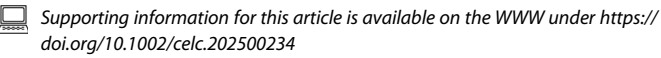
M. A. Khan, E. Bernalte, M. J. Whittingham, L. Slimani, K. K. L. Augusto, R. D. Crapnell, C. E. Banks
Faculty of Science and Engineering
Manchester Metropolitan University
Dalton Building, Chester Street, Manchester M1 5GD, Great Britain
E-mail: r.crapnell@mmu.ac.uk
c.banks@mmu.ac.uk

L. Slimani

K. K. L. Augusto

Department of Physical Measurements Sorbonne Paris North University Place du 8 Mai 1945, 93200 Saint-Denis, France

Institute of Chemistry
Federal University of Uberlândia
Campus Santa Mônica, Uberlândia, Minas Gerais 34800–902, Brazil



© 2025 The Author(s). ChemElectroChem published by Wiley-VCH GmbH. This is an open access article under the terms of the Creative Commons Attribution License, which permits use, distribution and reproduction in any medium, provided the original work is properly cited.

the electrochemically active surface area and improve electroanalytical performance.<sup>[1-3]</sup> Strategies to achieve changes in the electrode surface architecture have been seen previously through techniques such as lithography<sup>[4,5]</sup> and laser ablation.<sup>[6-8]</sup> More recently, different surface architectures have been produced for electrochemical systems through additive manufacturing, such as producing lattice structures.<sup>[9]</sup>

Additive manufacturing, colloquially referred to as 3D printing, is the name given to a group of manufacturing techniques that share the same principle of building a final physical object in a layer-by-layer fashion.[10-14] One additive manufacturing technique that has seen a surge in popularity and publications within the field of electrochemistry in the last decade is fused filament fabrication (FFF, also referred to as fused deposition modeling or FDM), due to its simplicity, low-cost of entry, and availability of commercial conductive filaments.[15-22] Using such conductive filaments, researchers were able to make useful items, exploring different shapes of working electrode, [23] lab equipment, [24] and accessories. [22,25,26] Although functional, items printed from the commercially available conductive filament were substandard and as such many strategies have been explored to improve their performance. This includes optimizing the design of the electrodes, [23,27,28] the printing parameters, [29-34] and post-print treatment, commonly referred to as 'activation'.[35-43] One method reported recently to improve electrochemical performance of additive manufactured electrodes is through surface patterning, where Miller et al.[28] produced electrodes with nine different surface morphologies, finding that electrodes with domed and flag patterns produced larger oxidation currents than others tested, which was attributed to the varying surface



roughness. Although informative, the definition of the surface patterns able to be obtained via FFF printing is quite large as it is dictated by the nozzle size, typically 0.4 or 0.6 mm, meaning that translating this reliably to typical working electrode sizes (2–3 mm) would be challenging. Even with improvements coming from this strategy, the electrochemical performance of the electrodes is inferior when compared to other commonly used electrodes due to the quality of the commercial filament used.

To overcome the limitations of commercial filaments, researchers have now began producing their own bespoke filaments.[44] The majority of this work has focused on poly(lactic acid) (PLA) based filaments, matching and out performing that of the commercial filament. Reported filament typically comes from the inclusion of a conductive carbon-based material such as carbon black, alongside the PLA and a plasticizing chemical to improve the low-temperature flexibility of the filament. Developments have focused on improving the performance through transitioning to mixed carbon material fillers[45-47] and on improving the sustainability of filament, such as using recycled PLA<sup>[48,49]</sup> or transitioning to bio-based plasticizers.<sup>[50–53]</sup> More recently, improvements have been sort through the addition of functional fillers, such as base metal powders<sup>[54,55]</sup> or metallic nanoparticles. [56-59] These advancements in materials have significantly improved the performance of additive manufactured electrodes, to the point that they are now a truly viable option alongside more classical working electrodes.

Although these PLA-based filaments now produce suitable electrochemical performance, these systems suffer from the inherent issues of the base polymer PLA, namely poor chemical stability<sup>[60]</sup> and solution ingress,<sup>[61]</sup> effectively making these electrodes single use items. To counter this, researchers have now reported high-performance conductive filament from a range of new materials, such as poly(ethylene terephthalate glycol) (PETg),<sup>[62,63]</sup> thermoplastic polyurethane (TPU),<sup>[64]</sup> and polypropylene (PP).<sup>[65,66]</sup> All these filaments demonstrated electrochemical performances that significantly improve that of commercially available conductive PLA, alongside bringing their own unique beneficial material properties.

It can be seen from the improvements reported above that additive manufacturing is now a staple within the arsenal of electrochemists. These advancements have been realized through clever engineering of design parameters, printer settings, and the development of bespoke filament. In this work, we look to manipulate a currently untapped potential source of improvement, the print bed. The print bed, also known as the build plate, is the flat surface on which the printer lays down the first layer of filament of any print. Through modification of the print bed via laser engraving, we look to produce unique microarchitectures. When the electrodes are printed, the material is therefore deposited into these patterns, giving the electrode matching surface architectures when removed. This approach enables enhancements in electrochemical performance, mainly through increased electroactive surface area, without the need of altering print files, consuming additional filament, or requiring extensive post-processing of the electrodes produced.

## 2. Results and Discussion

#### 2.1. Bed Patterning and Electrode Printing

To introduce novel microarchitectures on the electrode surfaces, the surface was printed face down onto print beds with the appropriate pattern engraved on it. The chosen patterns were parallel lines, crosses, circles, and sine waves, which were all compared to beds with no patterning for benchmarking. Note that these patterns are referred herein to 'Lines', 'Crosses', 'Circles', 'Waves', and 'None', respectively. These designs were then engraved onto the surfaces of the print beds using a laser cutter equipped with a 42 W  $\rm CO_2$  laser. Photographs of the final print beds, along with insets of the printed electrodes can be seen in **Figure 1**.

In each case seen in Figure 1, the inset electrode presents excellent definition for the desired surface architecture, confirming the reliability of the process. For the electrode printed on the unmodified print bed, lines can be also observed which are indicative of the rectilinear infill and surface pattern used in the slicing process. It is important to highlight that each electrode printed on a modified print bed was using an identical print file, with this rectilinear pattern being visible underneath the 'Lines' surface architecture. This infill pattern cannot be seen in any of the other electrodes due to the complexity of the surface architecture. This highlights the impact of engraving patterned microstructures on the print bed to drastically alter the surface of the additive manufactured electrode even when using identical electrode designs and print files and also using the same mass of filament. In this work, we will look to use three separate filaments. First, a bespoke conductive rPLA material containing 30 wt% carbon black (B-PLA) was chosen alongside the most commonly used commercial conductive PLA (C-PLA). These were chosen as PLA is the most commonly used print material and most reported conductive filament for electrode production in the literature. Lastly, a bespoke conductive PP filament containing 30 wt% carbon black (B-PP) was used. This was chosen as conductive PP has recently been reported, whereby the PP brings excellent chemical stability compared to PLA, having been shown to be stable and function for electrochemical processes in various organic solvents. As such, observing the effect these architectures have on a material with significantly different properties to PLA is of interest to the wider community. No commercially available conductive PP is available as hence was not used.

#### 2.2. Electrochemical Characterization

Once electrodes were printed on all 5 print surfaces out of each of the three materials (C-PLA, B-PLA, and B-PP) to be tested, they were subject to electrochemical characterization using cyclic voltammetric scan rate studies (5–500 mV s<sup>-1</sup>) against both outer and inner sphere redox probes. Initially, studies were performed against the near-ideal outer sphere redox probe hexaamineruthenium (III) chloride ([Ru(NH<sub>3</sub>)<sub>6</sub>]<sup>3+</sup>) as this allows for the best determination of the heterogeneous electron (charge) transfer rate constant ( $k^0$ ), electrochemically active area ( $A_e$ ), and allows for

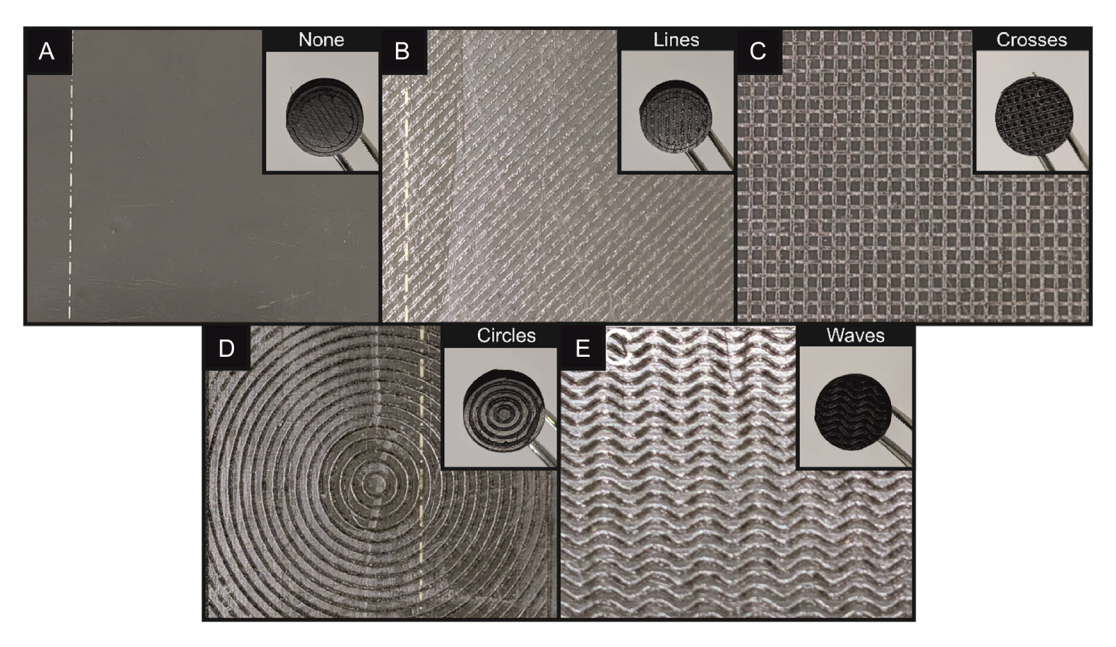


Figure 1. Images of the laser-engraved print beds, with inset images of the electrode surface after printing on the patterns A) None, B) Lines, C) Crosses, D) Circles, and E) Waves.

the best benchmarking against other literature reports of additive manufactured electrodes. [67,68] It is important to note that specific studies on the calculation of  $A_e$  validating this method for additive manufactured electrodes has not been published, but as a vast majority of reports in the field use this method, this allows for the best comparison between studies. In all cases, the expected single reduction and oxidation peaks corresponding to  $[Ru(NH_3)_6]^{3+}$  were obtained, with examples for the B-PP working electrodes with no additional surface architecture and a crosses surface architecture seen in **Figure 2**A and B with the same *y*-axis scale, respectively. Similar comparative scan rate studies using the no surface architecture and crosses surface architecture electrodes for the C-PLA and B-PLA can be seen in Figure S3, Supporting Information.

Within these figures, it can be seen that there is little variation between the electrodes with no surface architecture or crosses using both the C-PLA and the B-PLA; however, when utilizing the B-PP, there is a significant increase in the peak current values obtained. This is a trend consistently observed across the different surface architectures. The key electrochemical parameters obtained for each surface architecture printed in C-PLA, B-PLA, and B-PP are presented in Tables S1,S2, and 1, Supporting Information, respectively. First, when considering the peakto-peak separation ( $\Delta E_p$ ) and  $k^0$ , it can be seen that there is no significant change when introducing different surface architectures. For C-PLA, all  $\Delta E_p$  values fall between 168–187 mV and for the B-PP electrodes they are between 128-146 mV. A similar spread of values is observed for the B-PLA electrodes (77–90 mV); however, the reproducibility of the  $\Delta E_p$  values is significantly improved with this material, indicating a more consistent filament, but these values also do not show any particular trend. This result can be explained when considering that it is the intrinsic properties of the material the electrode is made from that affects the  $\Delta E_p$  and  $k^0$ , not the surface pattern. In contrast, when observing the peak reduction current and the calculated electrochemical area of the electrodes, there are significant changes when using the B-PP electrodes. A summary of the peak currents obtained for the reduction of [Ru(NH<sub>3</sub>)<sub>6</sub>]<sup>3+</sup> for each surface architecture and material are shown in Figure 2C. Importantly, for both the C-PLA and B-PLA electrodes, there is no significant change in the peak current when introducing different surface architectures; however, for the B-PP, there is an increase from 53.5  $\pm$  0.9  $\mu\text{A},$  for the electrode with no surface architecture, to 85.3  $\pm$  1.6  $\mu$ A, for the electrode with crosses surface architecture. This dramatic change when switching the base polymer of the working electrode is proposed to be due to the known solution ingress exhibited by PLA-based materials, [61] where it has been shown that significant amounts of solution are taken up into the polymeric structure of PLA electrodes. The ingress of the redox solution into the electrode negates any beneficial increase in electrochemical surface area. In comparison, B-PP does not show the same levels of solution ingress, [66] if any, and therefore, the introduction of surface architectures is expected to give a rise in electrochemically active surface area. This increase can be readily seen when considering Figure 2D, where once again no significant variation in the  $A_e$  can be seen for either of the PLA samples, but for every surface architecture introduced onto the B-PP electrodes, a significant increase in the  $A_e$  is observed. It is important to note that every electrode is printed using the same print file, with the same amount of filament used in every print; therefore, every electrode has the same theoretical geometric area. The effects are therefore not a result of adding more material to the interface, but rather through the patterns imparted on the electrode by the engraved print bed.

Following investigations with  $[Ru(NH_3)_6]^{3+}$ , studies with the commonly used inner sphere redox probe  $[Fe(CN)_6]^{4-/3-}$  were

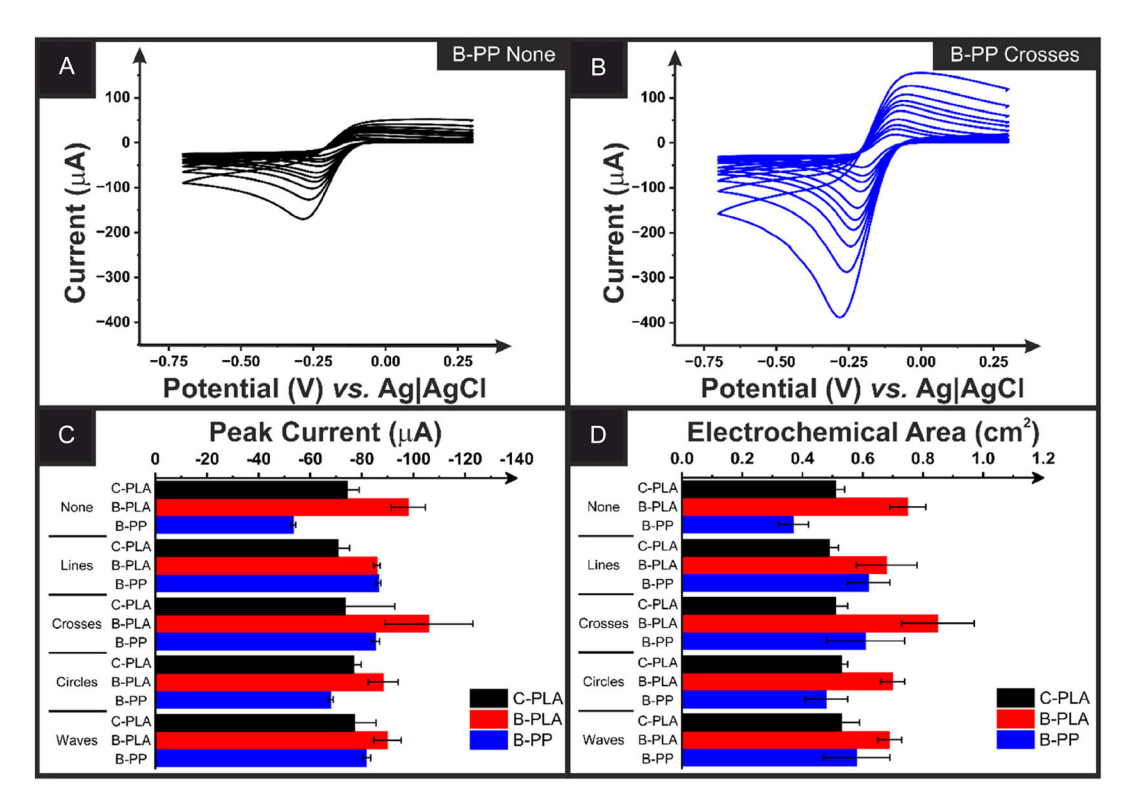


Figure 2. Scan rate studies (5–500 mV s<sup>-1</sup>) in  $[Ru(NH_3)_6]^{3+}$  (1 mM in 0.1 M KCl) performed with additive manufactured working electrodes printed with A) no additional surface architecture and B) crosses surface architecture, from B-PP filament with a nichrome coil counter electrode, and Ag|AgCl/KCl (3M) reference electrode. Bar charts showing the changes in C) peak reduction current (50 mV s<sup>-1</sup>) and D) electrochemical area for all surface architectures and materials used, measured in  $[Ru(NH_3)_6]^{3+}$  (1 mM in 0.1 M KCl) with a nichrome coil counter electrode, and Ag|AgCl/KCl (3M) reference electrode.

undertaken, as the majority of substances of interest for electroanalytical applications are not near-ideal outer sphere probes. The key electrochemical parameters of peak current and  $\Delta E_p$  are also present in Tables S1,S2, and 1, Supporting Information. Once again, there is no clear improvement in either of these parameters using either of the PLA-based materials when introducing surface architectures. It is noted that there is a significant improvement in the  $\Delta E_p$  for the circles surface architecture in B-PLA and peak current of the waves surface architecture in B-PLA, but these are attributed to random improvements in printing for that specific batch of electrodes as the improvement is not seen widely across all surface architecture. In contrast, for the B-PP, once again significant enhancements in the peak current

are obtained for all electrodes with a surface architecture when compared to the electrode with none. This once again supports that the ingress of solution into PLA-based electrodes negates any potential advantages through the introduction of surface architectures. If we now just consider B-PP electrodes, we can observe through **Table 1** that the largest improvement in peak current and  $A_e$  across both outer and inner sphere probes is with the crosses surface architecture. The improvement that is seen when introducing this crosses surface architecture compared to the other architectures and having none for both redox probes is highlighted in **Figure 3A** ([Ru(NH<sub>3</sub>)<sub>6</sub>]<sup>3+</sup>) and 3B ([Fe(CN)<sub>6</sub>]<sup>4-/3-</sup>).

When considering Figure 3, the significant improvement from the addition of the crosses surface architecture when using

Table 1. Summary of the key electrochemical values obtained using B-PP working electrodes. All experiments were performed in triplicate $(n = 3)$ .					
	Surface architecture				
	None	Lines	Crosses	Circles	Waves
-l <sub>p</sub> (μA) <sup>a)</sup>	53.5 ± 0.9	86.5 ± 0.9	85.3 ± 1.6	68.0 ± 0.9	81.8 ± 1.5
$\Delta E_p (mV)^{a)}$	146 $\pm$ 12	$130\pm2$	$128\pm12$	$132\pm6$	$133\pm1.4$
$k^0$ (x10 <sup>-3</sup> cm s <sup>-1</sup> ) <sup>b)</sup>	$1.5\pm0.2$	$1.6\pm0.1$	$1.5\pm0.2$	$1.6\pm0.1$	$1.6\pm0.1$
$A_e$ (cm <sup>2</sup> ) <sup>b)</sup>	$0.37\pm0.05$	$0.62\pm0.07$	$0.61\pm0.13$	$0.48\pm0.07$	$0.58\pm0.11$
I <sub>p</sub> (μΑ) <sup>c)</sup>	$25.6\pm6.9$	$40.3\pm6.4$	$78.5\pm4.4$	$63.6\pm3.5$	$46.7\pm6.5$
$\Delta E_{p} \ (mV)^{c)}$	$467\pm10$	$468\pm27$	$403\pm39$	$432\pm20$	457 $\pm$ 19

<sup>a)</sup>Key: Obtained in  $[Ru(NH_3)_6]^{3+}$  (1 mM in 0.1 M KCl) from cyclic voltammograms (25 mV s<sup>-1</sup>). <sup>b)</sup>Obtained in  $[Ru(NH_3)_6]^{3+}$  (1 mM in 0.1 M KCl) from scan rate studies (0.005–0.5 mV s<sup>-1</sup>). <sup>c)</sup>Obtained in  $[Fe(CN)_6]^{4-/3-}$  (1 mM in 0.1 M KCl) from cyclic voltammograms (25 mV s<sup>-1</sup>).

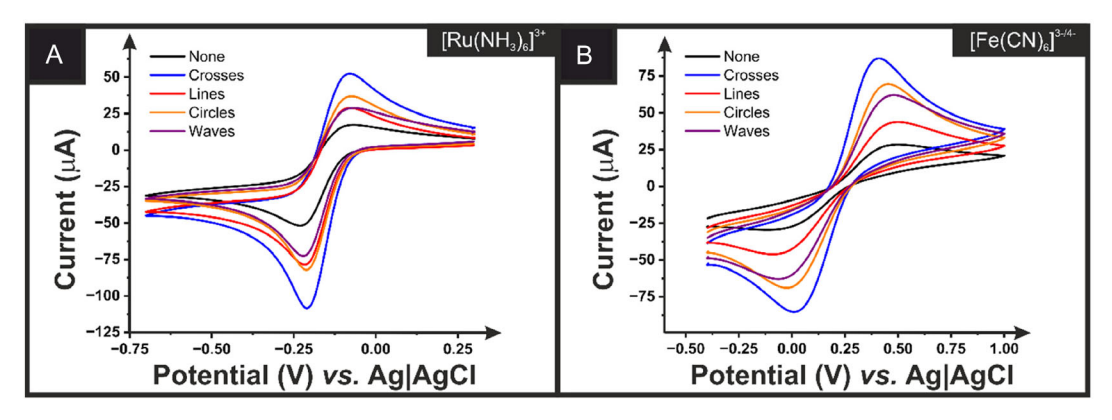


Figure 3. A) Cyclic voltammograms (25 mV s<sup>-1</sup>) of  $[Ru(NH_3)_6]^{3+}$  (1 mM in 0.1 M KCI) using working electrodes printed from B-PP with no surface architecture (black), crosses (blue), lines (red), circles (orange) and waves (purple). B) Cyclic voltammograms (25 mV s<sup>-1</sup>) of  $[Fe(CN)_6]^{4-/3-}$  (1 mM in 0.1 M KCI) using working electrodes printed from B-PP with no surface architecture (black), crosses (blue), lines (red), circles (orange), and waves (purple).

identical print files and the same amount of filament is stark. For the inner sphere probe  $[\text{Fe}(\text{CN})_6]^{4-/3-}$ , we observe an increase in the peak current (at 25 mV s $^{-1}$ ) from 25.6  $\pm$  6.9  $\mu\text{A}$  with no surface architecture to 78.5  $\pm$  4.4  $\mu\text{A}$ , highlighting the large increase in electrochemically active surface area achieved when using a print material that doesn't suffer from ingress. As the crosses surface architecture introduced the most consistent increase in performance in regard to the peak current, the electrodes with this surface architecture were next explored toward an electroanalytical application in comparison to an electrode with no additional surface architecture.

# 2.3. Electroanalytical Application of PP Electrodes

Working electrodes printed from the B-PP filament with no additional surface architecture and the crosses surface architecture were next applied toward electroanalytical applications. First, the response to both NADH and phenylephrine were examined with CV, Figure S4, which shows in both cases an improved response for the electrodes with a crosses surface architecture. Next, the electroanalytical determination of acetaminophen was explored using differential pulse voltammetry (DPV). [69,70]

Acetaminophen, commonly referred to as paracetamol, is a widely used and prescribed drug for pain relief and fever reduction due to its analgesic and antipyretic properties. It is an easily accessible drug, available in large amounts which can also lead to increased risk of excessive intake. Acetaminophen overdose has become one of the most common causes of emergency hospital admissions globally, with studies reporting in the United States alone, it leads to approximately 56,000 emergency department visits annually.<sup>[71]</sup> As such, the rapid and reliable detection of acetaminophen concentration is a vital analytical challenge.

To understand whether the improvements in electrochemical performance when adding the crosses surface architecture translated to the electroanalytical capabilities, the crosses and no surface architecture electrodes were applied to the detection of acetaminophen. Due to the enhanced sensitivity of the DPV process, the experimental set up was achieved as in Figure S2B, whereby the stamp was inverted and a droplet of solution added to the surface, with the reference and counter electrode inserted. This was done to minimize the contribution of the edges of the stamp, which possessed slower electron transfer kinetics. The voltammograms obtained for the addition of acetaminophen (5–60  $\mu$ M) to the electrode with the crosses surface architecture can be seen in **Figure 4**A.

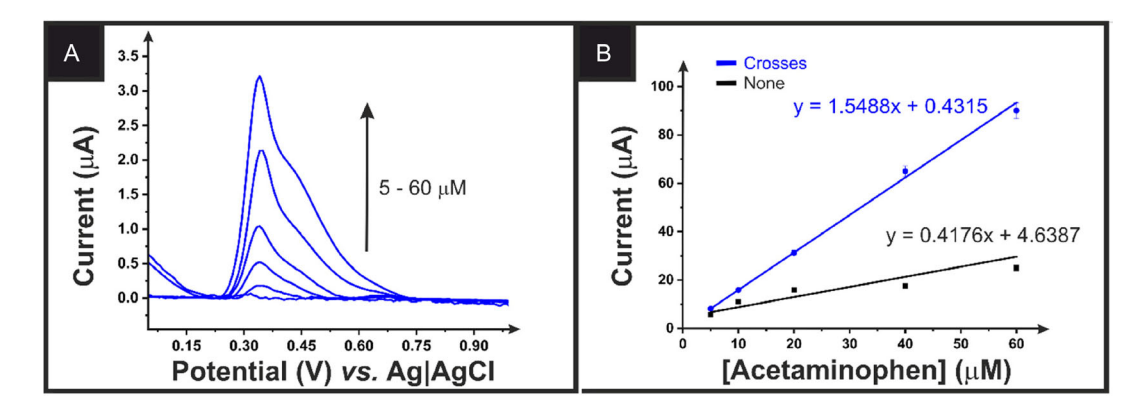


Figure 4. A) Differential pulse voltammograms for the detection of acetaminophen (5–60  $\mu$ M) in 0.1 M PBS (pH = 7.4) using B-PP electrodes with the crosses surface architecture. B) Calibration plots corresponding to the detection of acetaminophen using B-PP electrodes with no surface architecture (black) and crosses surface architecture (blue).

**Table 2.** Recovery values calculated for the detection of acetaminophen within real river water samples.

	·	
Sample	Surface architecture	Recovery [%]
1	None	113.0
	Crosses	91.1
2	None	97.8
	Crosses	102.7
3	None	116.2
	Crosses	94.9

Even with this experimental set up, a slight splitting of the acetaminophen oxidation peak was observed, with the peak at  $\approx +0.32$  V attributed to the oxidation at the patterned surface. Using this peak, calibration curves were obtained for both the none and crosses surface architecture electrodes, Figure 4B. It can be seen that a large increase in peak current and sensitivity was obtained when using the electrode with the crosses surface architecture. The sensitivity obtained for the crosses surface architecture was 1.55  $\mu A$   $\mu M^{-1}$ , over three times larger than the  $0.42~\mu A~\mu M^{-1}$ , obtained for the electrode with no additional surface architecture. The limit of detection (LOD) and limit of quantification (LOQ) for each system was calculated using 3 and 10 times the standard deviation of the blank divided by the slope of the curve. Through this, the electrodes with the crosses surface architecture produced LOD and LOQ values of 0.80 and 2.65 μM, respectively, compared to 1.25 and 4.12 µM for the electrode with no additional surface architecture. These values compared well to others reported in the literature, Table S3, showing significant improvements on other additive manufactured electrodes.

Finally, both the electrode with none and the crosses surface architecture were applied toward the detection of acetaminophen within real river water samples, spiked with 20  $\mu$ M of the target. The results for these samples are presented in **Table 2**.

It can be seen from Table 2 that both electrodes produced good recovery values for the determination of acetaminophen in river water samples. The electrodes with the crosses surface architecture produced the most accurate and consistent results across the three samples showing recovery rates between 91.1 and 102.7%. This once again highlights the beneficial improvements in performance that can be obtained through introducing novel surface architectures onto electrodes.

# 3. Conclusions

In this work, we present a new way to introduce novel micron sized surface architectures onto the surface of additive manufactured working electrodes. Through laser engraving the poly(etherimide) print beds, unique and bespoke patterns were able to be deposited, onto which the additive manufactured electrodes could be printed. Four different micron sized surface architectures (lines, crosses, waves, and circles) were successfully manufactured on the surface of commercial conductive PLA, bespoke PLA, and bespoke PP electrodes. Through

electrochemical characterization against inner and outer-sphere redox probes, it was seen that the surface architectures had no significant effect on the PLA-based electrodes, which is proposed to be due to solution ingress nullifying the enhanced surface area contribution. In contrast, for PP-based electrodes, the introduction of additional surface architectures produced significant improvements in the electrochemical performance when compared to unmodified electrodes. It was seen that the crosses surface architecture produced the most improved performance, with an increase in  $[Ru(NH_3)_6]^{3+}$  peak current from 53.5  $\pm$  0.9  $\mu A$  for the electrode with no pattern to 85.3  $\pm$  1.6  $\mu$ A for the crosses. This was also seen for  $[Fe(CN)_6]^{4-/3-}$ , where an increase in the peak current (at 25 mV s $^{-1}$ ) from 25.6  $\pm$  6.9  $\mu A$  with no pattern to 78.5  $\pm$  4.4  $\mu A$  with crosses was observed. This improvement was also seen for the electroanalytical performance toward acetaminophen detection, with the cross architecture producing a sensitivity of 1.55  $\mu A$   $\mu M^{-1}$ , over three times larger than the  $0.42 \,\mu\text{A} \,\mu\text{M}^{-1}$  seen for the electrode with no addition architecture. This improvement was also seen within the LOD and LOQ values obtained, with the crosses surface architecture producing values of 0.80 and 2.65  $\mu$ M, respectively, compared to 1.25 and 4.12  $\mu$ M for the electrode with no additional surface architecture. This work highlights a new way to introduce novel bespoke architectures onto the surface of additive manufactured electrodes to enhance the electrochemical performance without changing the amount of filament used.

# 4. Experimental Section

#### Chemicals

All chemicals used throughout this work were used as received without any further purification. All aqueous solutions were prepared with deionized water of a measured resistivity not <18.2 M $\Omega$  cm, sourced from a Milli-Q Integral 3 system from Millipore UK (Watford, UK). Hexaammineruthenium (III) chloride (>98%), castor oil, potassium ferricyanide (99%), potassium ferrocyanide (98.5–102%), sodium hydroxide (>98%), potassium chloride (99.0–100.5%), acetaminophen ( $\geq$ 99%), and phosphate-buffered saline (PBS) tablets were purchased from Merck (Gillingham, UK). Recycled poly(lactic acid) (rPLA) was purchased from Gianeco (Turin, Italy). Polypropylene (PP, Sabic CX03–81 Natural 00900) was purchased from Hardie Polymers (Glasgow, UK). Commercial conductive CB/PLA filament (1.75 mm, ProtoPasta, Vancouver, Canada) was purchased from Farnell (Leeds, UK). Real river water samples were collected following the EPA guidelines<sup>[72]</sup> (Approximate location: 53.601192, -2.301887).

#### **Production of Laser-Engraved Print Beds**

To create the engraved beds, the open-source Prusa Research build sheet files were acquired as a starting point. These can be sourced from the Prusa GitHub for the Mk.52 Heatbed. The steel sheet .dxf file was then imported into Adobe Illustrator, and four patterns were created in  $10 \times 10$  cm² squares: 1 mm Grid; 1 mm Diagonal Lines; 2 mm Circle with 1 mm Offsets; and repeating sine waves with 1 mm offset, 5 mm wavelength and 0.8 mm amplitude, Figure S1, Supporting Information.

The .dxf files were then engraved onto the Prusa beds using a Glowforge Pro laser cutter, which uses a 45 W CO $_2$  laser. It was found that each print sheet required very slightly different power/speed settings to engrave, possibly due to the factory variations in poly(etherimide) (PEI) thickness applied to the plates. The laser was set to 'cut' mode instead of 'engrave' mode, in order to have the laser trace the paths rather than raster (scan) engrave them as images. For a practical replication of this process, the authors recommend creating a small test pattern starting at around 50% laser power and 500 mm s $^{-1}$  cut speed, adjusting these settings as needed until the engravings are crisp and the PEI is not burned. Note that slight charring is normal, but this can be cleaned off using isopropyl alcohol and a lint-free cleaning cloth.

A batch of electrodes was first printed onto the build sheets to assess feasibility, and once confirmed, four separate build plates were created—one for each pattern—to speed up production of the additive manufactured electrodes for testing.

#### **Recycled Filament Production**

All polymers were dried in an oven at 60 °C for a minimum of 2.5 h before use to remove any residual water. The bespoke PLA was prepared through the addition of appropriate amounts of rPLA (60 wt%), castor oil (10 wt%),<sup>[50]</sup> and carbon filler (30 wt%) in a chamber of 63 cm<sup>3</sup>. The bespoke PP was prepared through the addition of appropriate amounts of PP (70 wt%) and carbon filler (30 wt%) in a chamber of 63 cm<sup>3</sup>. The compounds were mixed using a Thermo Haake Polydrive dynameter fitted with a Thermo Haake Rheomix 600 (Thermo-Haake, Germany) at 190 °C for rPLA and 210 °C for PP, respectively, with Banbury rotors working at 70 rpm for 5 min. The resulting polymer composites were allowed to cool to room temperature before being granulated to create a finer particle size using a Rapid Granulator 1528 (Rapid, Sweden). The polymer composites were collected and processed through the hopper of a EX2 extrusion line (Filabot, VA, United States). The EX2 was set up with a single screw with a heat zone of 190 °C for rPLA and 210 °C for PP. The molten polymer was extruded from a 1.75 mm die head, pulled along an Airpath cooling line (Filabot, VA, United States) and collected on a spool. After which the filament was then ready to use for additive manufacturing.

#### Additive Manufacturing of the Electrodes

All computer designs and 3MF files in this manuscript were produced using Fusion 360 (Autodesk, CA, United States). These files were sliced and converted to GCODE files in PrusaSlicer (Prusa Research, Prague, Czech Republic). The additive manufactured electrodes were produced using FFF technology on a Prusa i3 MK3S+ (Prusa Research, Prague, Czech Republic). All additive manufactured electrodes were printed using identical printer components and printing parameters, namely a 0.6 mm nozzle with a nozzle temperature of 215 °C (PLA) or 240 °C (PP), 100% rectilinear infill, [29] 0.2 mm layer height, and print speed of 35 mm s<sup>-1</sup>. Electrodes were printed on a laser-engraved smooth PEI steel sheet heated to 50 °C for PLA filaments or an identical sheet modified with Magigoo PP adhesive glue set to 100 °C for PP filaments. To create the print files, the custom build sheets were loaded into the Prusa i3 Mk3s+, and the nozzle was jogged manually until centered in each of the patterns. These coordinates were noted, and the 3D models were centered accordingly in Prusa Slicer software, so that the patterns were centered on the electrode surfaces. Identical additive manufactured electrodes were used throughout this work for all filaments, printed in the shape of a stamp, Figure S2, Supporting Information, which allowed for the working electrode surface to be printed face down onto the laserengraved print bed, but also keeping the connection length as short as possible.<sup>[27]</sup> It is important to note that every electrode had the same design and used the same amount of filament. No additional filament was added in to make the surface patterns; this was simply due to the first layer being deposited onto a patterned surface.

#### **Electrochemical Experiments**

All electrochemical experiments were performed on an Autolab 100N potentiostat controlled by NOVA 2.1.7 (Utrecht, The Netherlands). Identical additive manufactured electrodes were used throughout this work for all filaments alongside an external commercial Agl AgCl/KCl (3M) reference electrode with a nichrome wire counter electrode. All solutions of  $[Ru(NH_3)_6]^{3+}$  were purged of  $O_2$  thoroughly using  $N_2$  prior to any electrochemical experiments. Solutions of  $[Fe(CN)_6]^{4-/3-}$  were prepared in the same way without the need of further degassing.

Activation of the additive manufactured electrodes was performed, where applicable, electrochemically in NaOH (0.5 M), as described in the literature. [74] Briefly, the additive manufactured electrodes were connected as the working electrode in conjunction with a nichrome wire coil counter and Ag|AgCl/KCl (3 M) reference electrodes and placed in a solution of 0.5 M NaOH. Chronoamperometry was used to activate the additive manufactured electrodes by applying a set voltage of  $\pm 1.4$  V for 200 s, followed by applying  $\pm 1.0$  V for 200 s. The additive manufactured electrodes were then thoroughly rinsed with deionized water and dried under compressed air before further use. It should be noted that all PP electrodes were treated in this way no matter the experiment, as this process is used to remove the adhesive used in the printing process.

The electroactive area of the electrode,  $A_{er}$  is calculated using the Randles-Ševćik equation at no-standard conditions for quasi- (1) and irreversible (21) electrochemical processes when appropriate<sup>[75]</sup>

$$I_{p,f}^{quasi} = \pm 0.436 \, nFA_{real} C \, \sqrt{\frac{nFDv}{RT}} \tag{1}$$

$$I_{p,f}^{irrev} = \pm 0.496 \sqrt{\alpha + n'} \, nFA_{real} C \sqrt{\frac{nFDv}{RT}}$$
 (2)

where, in all cases, n is the number of electrons in the electrochemical reaction,  $I_{p,f}$  is the voltammetric current (analytical signal) using the first peak of the electrochemical process, F is the Faraday constant  $(C \text{ mol}^{-1})$ , v is the applied voltammetric scan rate  $(V \text{ s}^{-1})$ , R is the universal gas constant, T is the temperature in Kelvin,  $A_{real}$  is the electroactive area of the electrode (cm<sup>2</sup>), and D is the diffusion coefficient (cm<sup>2</sup> s<sup>-1</sup>), which for [Ru(NH<sub>3</sub>)<sub>6</sub>]<sup>3+</sup> is used as  $9.1 \times 10^{-6}$  cm s<sup>-1</sup>, and  $\alpha$  is the transfer coefficient (usually assumed to be close to 0.5) and n' is the number of electrons transferred before the rate determining step. It should be noted that for equations (1) and (2) to hold, the electrode should be flat and nonporous, whereas AMEs are made from different carbons, polymers, and plasticizers, and, also, in this paper, they possess microsurface architectures. However, as seen previously with screen-printed electrodes, which also have an heterogeneous surface morphology, at slow scan rates, the diffusion layer is larger than the micro-features. [67] As such, the kinetics are dominated by the edge plane features of the conductive materials, meaning over the timescales of the cyclic voltammetric experiments, the equations hold.<sup>[76,77]</sup> In this way, as  $[Ru(NH_3)_6]^{3+}$  is a near-ideal outer sphere redox probe, which is only dependent on the electrodes electronic structure, it allows us to gain the closest estimations of the real electrode area.



DPV was used for the determination of acetaminophen applying a potential window from 0 to +1.3 V, with a step potential of 8 mV, modulation amplitude of 50 mV, modulation time of 0.05 s, and interval time of 0.5 s. These experiments were carried out in a drop of solution (200  $\mu L)$  deposited onto the patterned additive manufactured working electrode with reference and counter electrodes strategically placed within the drop of solution (Figure S2, Supporting Information).

# **Acknowledgements**

The authors would like to thank Aquacheck for the partial funding of MK's PhD studies. E.B. would like to thank Horizon Europe (101137990).

# Conflict of Interest

The authors declare no conflict of interest.

# Data Availability Statement

The data that support the findings of this study are available from the corresponding author upon reasonable request.

**Keywords:** 3D-printing  $\cdot$  acetaminophen  $\cdot$  additive manufacturing  $\cdot$  electroanalysis  $\cdot$  electrochemistry  $\cdot$  laser engraving  $\cdot$  poly(lactic acid)  $\cdot$  polypropylene

- [1] Q. Cao, D. K. Hensley, N. V. Lavrik, B. J. Venton, Carbon 2019, 155, 250.
- [2] Q. Cao, Z. Shao, D. K. Hensley, N. V. Lavrik, B. J. Venton, *Langmuir* 2021, 37, 2667.
- [3] K. R. Ward, N. S. Lawrence, R. S. Hartshorne, R. G. Compton, *Phys. Chem. Chem. Phys.* 2012, 14, 7264.
- [4] H. Sugimura, O. Takai, N. Nakagiri, J. Electroanal. Chem. 1999, 473, 230.
- [5] A. Baradoke, J. Juodkazyte, I. Masilionis, A. Selskis, R. Pauliukaite, R. Valiokas, *Microelectron. Eng.* 2019, 208, 39.
- [6] N. Dunlap, D. B. Sulas-Kern, P. J. Weddle, F. Usseglio-Viretta, P. Walker, P. Todd, D. Boone, A. M. Colclasure, K. Smith, B. J. T. de Villers, J. Power Sources 2022, 537, 231464.
- [7] M. A. A. Rehmani, K. Lal, A. Shaukat, K. M. Arif, Sci. Rep. 2022, 12, 6928.
- [8] L. M. Tender, R. L. Worley, H. Fan, G. P. Lopez, Langmuir 1996, 12, 5515.
- [9] P. Wuamprakhon, R. D. Crapnell, E. Sigley, N. J. Hurst, R. J. Williams, M. Sawangphruk, E. M. Keefe, C. E. Banks, Adv. Sustainable Syst. 2023, 7, 2200407.
- [10] M. Attaran, J. Serv. Sci. Manag. 2017, 10, 189.
- [11] M. Attaran, Bus. Horiz. 2017, 60, 677.
- [12] I. Gibson, D. Rosen, B. Stucker, M. Khorasani, D. Rosen, B. Stucker, M. Khorasani, Additive Manufacturing Technologies, Springer Nature, Switzerland AG 2021.
- [13] K. R. Ryan, M. P. Down, C. E. Banks, Chem. Eng. J. 2021, 403, 126162.
- [14] K. V. Wong, A. Hernandez, Int. Sch. Res. Notices 2012, 2012, 208760.
- [15] A. Ambrosi, M. Pumera, Chem. Soc. Rev. 2016, 45, 2740.
- [16] M. P. Browne, E. Redondo, M. Pumera, Chem. Rev. 120 2020, 2783.
- [17] R. M. Cardoso, C. Kalinke, R. G. Rocha, P. L. Delos Santos, D. P. Rocha, P. R. Oliveira, B. C. Janegitz, J. A. Bonacin, E. M. Richter, R. A. Munoz, Anal. Chim. Acta 2020, 1118, 73.
- [18] M. Choińska, V. Hrdlička, H. Dejmková, J. Fischer, L. Míka, E. Vaněčková, V. Kolivoška, T. Navrátil, Biosensors 2022, 12, 308.
- [19] J. Hengsteler, K. A. Kanes, L. Khasanova, D. Momotenko, Ann. Rev. Anal. Chem. 2023, 16, 71.
- [20] B. Huner, M. Kıstı, S. Uysal, I. N. Uzgoren, E. Ozdogan, Y. O. Suzen, N. Demir, M. F. Kaya, ACS Omega 2022, 7, 40638.

- [21] S. Rajesh, A. S. Kumawat, Ionics 2024, 30, 677.
- [22] M. J. Whittingham, R. D. Crapnell, E. J. Rothwell, N. J. Hurst, C. E. Banks, *Talanta Open* 2021, 4, 100051.
- [23] A. G.-M. Ferrari, N. J. Hurst, E. Bernalte, R. D. Crapnell, M. J. Whittingham, D. A. Brownson, C. E. Banks, *Analyst* 2022, 147, 5121.
- [24] M. J. Whittingham, R. D. Crapnell, C. E. Banks, Anal. Chem. 2022, 94, 13540.
- [25] H. Agrawaal, J. Thompson, Talanta Open 2021, 3, 100036.
- [26] B. Gross, S. Y. Lockwood, D. M. Spence, Anal. Chem. 2017, 89, 57.
- [27] R. D. Crapnell, A. G.-M. Ferrari, M. J. Whittingham, E. Sigley, N. J. Hurst, E. M. Keefe, C. E. Banks, Sensors 2022, 22, 9521.
- [28] C. Miller, O. Keattch, R. S. Shergill, B. A. Patel, Analyst 2024, 149, 1502.
- [29] E. Bernalte, R. D. Crapnell, O. M. Messai, C. E. Banks, ChemElectroChem 2024, 11, e202300576.
- [30] R. G. Rocha, D. L. Ramos, L. V. de Faria, R. L. Germscheidt, D. P. dos Santos, J. A. Bonacin, R. A. Munoz, E. M. Richter, J. Electroanal. Chem. 2022, 925, 116910.
- [31] R. S. Shergill, P. Bhatia, L. Johnstone, B. A. Patel, ACS Sustainable Chem. Ena. 2023, 12, 416.
- [32] R. S. Shergill, C. L. Miller, B. A. Patel, Sci. Rep. 2023, 13, 339.
- [33] R. S. Sherqill, B. A. Patel, ChemElectroChem 2022, 9, e202200831.
- [34] J. S. Stefano, C. Kalinke, R. G. da Rocha, D. P. Rocha, V. A. O. P. da Silva, J. A. Bonacin, L. Angnes, E. M. Richter, B. C. Janegitz, R. A. A. Muñoz, Anal. Chem. 2022, 94, 6417.
- [35] M. P. Browne, F. Novotny, Z. Sofer, M. Pumera, ACS Appl. Mater. Interfaces 2018, 10, 40294.
- [36] M. S. Carvalho, R. G. Rocha, A. B. Nascimento, D. A. Araújo, T. R. Paixão, O. F. Lopes, E. M. Richter, R. A. Muñoz, Electrochim. Acta 2024, 506, 144995.
- [37] P. L. dos Santos, V. Katic, H. C. Loureiro, M. F. dos Santos, D. P. dos Santos, A. L. Formiga, J. A. Bonacin, Sens. Actuators B: Chem. 2019, 281, 837.
- [38] C. Kalinke, N. V. Neumsteir, G. de Oliveira Aparecido, T. V. de Barros Ferraz, P. L. Dos Santos, B. C. Janegitz, J. A. Bonacin, *Analyst* 2020, 145, 1207.
- [39] J. F. Pereira, R. G. Rocha, S. V. Castro, A. F. Joao, P. H. Borges, D. P. Rocha, A. de Siervo, E. M. Richter, E. Nossol, R. V. Gelamo, Sens. Actuators B: Chem. 2021, 347, 130651.
- [40] E. Redondo, J. Muñoz, M. Pumera, Carbon 2021, 175, 413.
- [41] D. P. Rocha, R. G. Rocha, S. V. Castro, M. A. Trindade, R. A. Munoz, E. M. Richter, L. Angnes, Electrochem. Sci. Adv. 2022, 2, e2100136.
- [42] R. S. Shergill, F. Perez, A. Abdalla, B. A. Patel, J. Electroanal. Chem. 2022, 905, 115994.
- [43] H. A. Silva-Neto, M. Santhiago, L. C. Duarte, W. K. Coltro, Sens. Actuators B: Chem. 2021, 349, 130721.
- [44] R. D. Crapnell, C. Kalinke, L. R. G. Silva, J. S. Stefano, R. J. Williams, R. A. A. Munoz, J. A. Bonacin, B. C. Janegitz, C. E. Banks, *Mater. Today* 2023, 71, 73.
- [45] I. V. Arantes, R. D. Crapnell, E. Bernalte, M. J. Whittingham, T. R. Paixão, C. E. Banks, Anal. Chem. 2023, 95, 15086.
- [46] K. K. Augusto, R. D. Crapnell, E. Bernalte, S. Zighed, A. Ehamparanathan, J. L. Pimlott, H. G. Andrews, M. J. Whittingham, S. J. Rowley-Neale, O. Fatibello-Filho, *Microchim. Acta* 2024, 191, 375.
- [47] R. D. Crapnell, I. V. Arantes, J. R. Camargo, E. Bernalte, M. J. Whittingham, B. C. Janegitz, T. R. Paixão, C. E. Banks, *Microchim. Acta* 2024, 191, 96.
- [48] R. D. Crapnell, E. Sigley, R. J. Williams, T. Brine, A. G.-M. Ferrari, C. Kalinke, B. C. Janegitz, J. A. Bonacin, C. E. Banks, ACS Sustainable Chem. Eng. 2023, 11, 9183.
- [49] E. Sigley, C. Kalinke, R. D. Crapnell, M. J. Whittingham, R. J. Williams, E. M. Keefe, B. C. Janegitz, J. A. Bonacin, C. E. Banks, ACS Sustainable Chem. Eng. 2023, 11, 2978.
- [50] R. D. Crapnell, I. V. Arantes, M. J. Whittingham, E. Sigley, C. Kalinke, B. C. Janegitz, J. A. Bonacin, T. R. Paixão, C. E. Banks, *Green Chem.* 2023, 25, 5591.
- [51] J. P. C. Silva, R. G. Rocha, G. P. Siqueira, C. F. Nascimento, M. H. Santana, E. Nossol, E. M. Richter, I. S. da Silva, R. A. Muñoz, *Microchim. Acta* 2025, 192
- [52] L. R. Silva, L. V. Bertolim, J. S. Stefano, J. A. Bonacin, E. M. Richter, R. A. Munoz, B. C. Janegitz, Electrochim. Acta 2025, 513, 145566.
- [53] R. D. Crapnell, I. V. Arantes, E. Bernalte, E. Sigley, G. C. Smith, T. R. Paixão, C. E. Banks, *Analyst* 2025, 150, 2702.
- [54] E. Koukouviti, A. Economou, C. Kokkinos, Adv. Funct. Mater. 2024, 34, 2402094.
- [55] E. C. Okpara, R. D. Crapnell, E. Bernalte, O. B. Wojuola, C. E. Banks, Electroanalysis 2025, 37, e12019.
- [56] E. Bernalte, K. K. Augusto, R. D. Crapnell, H. G. Andrews, O. Fatibello-Filho, C. E. Banks, RSC Appl. Interfaces 2025, 2, 439.

# Research Article doi.org/10.1002/celc.202500234



- [57] E. Bernalte, R. D. Crapnell, R. El Azizi, K. K. Augusto, C. E. Banks, Appl. Mater. Today 2025, 42, 102578.
- [58] K. K. Augusto, E. Bernalte, R. D. Crapnell, H. G. Andrews, O. Fatibello-Filho, C. E. Banks, J. Environ. Chem. Eng. 2025, 13, 116446.
- [59] K. K. Augusto, R. D. Crapnell, E. Bernalte, H. G. Andrews, O. Fatibello-Filho, C. E. Banks, *Green Chem.* 2025, 27, 6869.
- [60] K. S. Erokhin, E. G. Gordeev, V. P. Ananikov, Sci. Rep. 2019, 9, 20177.
- [61] R. J. Williams, T. Brine, R. D. Crapnell, A. G.-M. Ferrari, C. E. Banks, *Mater. Adv.* 2022, 3, 7632.
- [62] J. R. Camargo, R. D. Crapnell, E. Bernalte, A. J. Cunliffe, J. Redfern, B. C. Janegitz, C. E. Banks, Appl. Mater. Today 2024, 39, 102285.
- [63] R. D. Crapnell, E. Bernalte, E. Sigley, C. E. Banks, *RSC Adv.* **2024**, *14*, 8108.
- [64] A. C. Oliveira, E. Bernalte, R. D. Crapnell, M. J. Whittingham, R. A. Munoz, C. E. Banks, Appl. Mater. Today 2025, 42, 102597.
- [65] B. Ferreira, R. D. Crapnell, E. Bernalte, T. R. Paixão, C. E. Banks, *Electrochim. Acta* 2025, 515, 145680.
- [66] D. L. Ramos, R. D. Crapnell, R. Asra, E. Bernalte, A. C. Oliveira, R. A. Muñoz, E. M. Richter, A. M. Jones, C. E. Banks, ACS Appl. Mater. Interfaces 2024, 16, 56006
- [67] A. G. í.-M. Ferrari, C. W. Foster, P. J. Kelly, D. A. Brownson, C. E. Banks, Biosensors 2018, 8, 53.

- [68] R. D. Crapnell, C. E. Banks, Talanta Open 2021, 4, 100065.
- [69] W. Boumya, N. Taoufik, M. Achak, N. Barka, J. Pharm. Anal. 2021, 11, 138.
- [70] L. M. Melo, K. A. Souza, J. E. Lopes, R. A. Muñoz, J. L. Costa, W. T. D. Santos, Anal. Chim. Acta 2024, 1333, 343243.
- [71] S. Agrawal, B. Khazaeni, Acetaminophen Toxicity 2017.
- [72] U.S.E.P. Agency, Quick Guide to Drinking Water Sample Collection 2005.
- [73] P. Research, Prusa 3D Heatbed MK52 Magnetic 2025.
- [74] E. M. Richter, D. P. Rocha, R. M. Cardoso, E. M. Keefe, C. W. Foster, R. A. Munoz, C. E. Banks, *Anal. Chem.* **2019**, *91*, 12844.
- [75] A. J. Bard, L. R. Faulkner, H. S. White, Electrochemical Methods: Fundamentals and Applications, John Wiley & Sons, New Jersey, USA 2022.
- [76] R. G. Compton, C. E. Banks, *Understanding Voltammetry*, World Scientific, Imperial College Press, London, UK 2018.
- [77] T. J. Davies, R. R. Moore, C. E. Banks, R. G. Compton, J. Electroanal. Chem. 2004, 574, 123.

Manuscript received: June 11, 2025 Revised manuscript received: August 14, 2025 Version of record online: